Journal of Power Sources 196 (2011) 2403–2409

Contents lists available at ScienceDirect

Journal of Power Sources

journal homepage: www.elsevier.com/locate/jpowsour

Electrochemically activated carbon micro-electrode arrays for electrochemical micro-capacitors

Majid Beidaghi, Wei Chen, Chunlei Wang*

Department of Mechanical and Materials Engineering, Florida International University, 10555 W. Flagler St., EC 3463, Miami, FL 33174, USA

ARTICLE INFO

Article history:
Received 6 July 2010
Received in revised form 6 September 2010
Accepted 20 September 2010
Available online 29 September 2010

Keywords:
Carbon-microelectromechanical systems (C-MEMS)
Electrochemical activation
Electrochemical capacitor
Cyclic voltammetry
Charge/discharge

ABSTRACT

Interdigitated carbon micro-electrode arrays for micro-capacitors are fabricated through the carbon microelectromechanical systems (C-MEMS) technique which is based on the carbonization of patterned photoresist. To improve the capacitive behavior, electrochemical activation is performed on carbon micro-electrode arrays. Cyclic voltammetry (CV) and galvanostatic charge–discharge results demonstrate that the electrochemical activation effectively increases the capacitance of the micro-electrode arrays by three orders of magnitude. Although the charge–discharge experiments show the non-ideal behavior of micro-capacitors, the specific geometric capacitance reaches as high as 75 mF cm^{-2} at a scan rate of 5 mV s^{-1} after electrochemical activation for 30 min. The capacitance loss is less than 13% after 1000 CV cycles. These results indicate that electrochemically activated C-MEMS micro-electrode arrays are promising candidates for on-chip electrochemical micro-capacitor application.

1. Introduction

Development of miniaturized electronic systems has derived the demand for miniaturized power sources that can be integrated into such systems. Several kinds of micron-sized power sources such as micro-batteries [1], micro-fuel cells [2], and energy harvesters [3] have been developed in recent years. However, for the applications that require high power, there is a need for miniaturized electrochemical capacitors (micro-capacitors) [4]. Electrochemical micro-capacitors with high power density can be coupled with energy harvesting devices to store the generated energy. Moreover, they can also be paired with micro-batteries to provide the peak power and improve the cycle lifetime. Based on the charge storage mechanism, electrochemical capacitors (ECs) can be divided into electric double layer capacitors (EDLCs) and pseudo-capacitors [5]. The former utilizes interfacial double layer capacitance of various types of carbon materials to store electric charge. The latter, the pseudo-capacitor or redox capacitor, uses fast and reversible surface or near-surface redox reactions for charge storage. The active materials of pseudo-capacitors include transition metal oxides and conductive polymers [5,6]. Micro-capacitors of both types have been reported in the literature [4,7–10]. For example, Lim et al. [4] reported that a thin film EC based on pseudo-capacitive ruthenium oxide (RuO_2) and Lipon solid electrolyte delivered a volumetric capacitance of about 38 mF cm^{-2} μm^{-1}, however its capacitance dropped by 53% after 500 cycles. Electrochemical micro-capacitor based on conductive polymer was first reported by Sung et al., who fabricated polypyrrole (Ppy) micro-electrodes by electrochemical deposition on interdigitated gold electrodes [7]. More recently, Sun and Chen [8] reported the fabrication of three-dimensional (3D) Ppy electrode architectures for micro-capacitors with geometric capacitance of the 27 mF cm^{-2} (normalized by the footprint area) at 1 mA cm^{-2} current density. On the other hand, EDLCs usually have higher rate capability, higher power density, and an extended cyclic life compared to pseudo-capacitors [6]. In recent years, some efforts to fabricate micro-scale EDLCs are reported [9,10]. For example, fabrication of printable thin film ECs with single-walled carbon nanotubes as electroactive materials has been reported by Kaempgen et al., where the estimated capacitance of the fabricated cell was 1.1 mF cm^{-2}, in a potential window of 0–1.0 V [9]. In addition, ECs from inkjet printing of activated carbon powders on interdigitated gold current collectors reached the maximum cell capacitance of 2.1 mF cm^{-2} at a low scan rate of 1 mV s^{-1} [10].

In this study, the carbon electrochemical systems (C-MEMS) technique was used to fabricate micro-electrodes for electrochemical capacitors. Furthermore, for the first time, an activation method was employed to improve electrochemical properties of C-MEMS electrodes. The C-MEMS technique is a simple and reproducible process for fabricating various glassy carbon structures with micro patterns, in which patterned photoresist is pyrolyzed and converted into carbon under high temperatures in an inert atmosphere

* Corresponding author. Tel.: +1 305 348 1217; fax: +1 305 348 1932.
E-mail address: wangc@fiu.edu (C. Wang).

0378-7753/$ – see front matter © 2010 Elsevier B.V. All rights reserved.
doi:10.1016/j.jpowsour.2010.09.050

[11–13]. The advantages of using C-MEMS to fabricate micro-capacitor electrodes are that this technique is compatible with other MEMS processes and allows the possibility to fabricate 3D glassy carbon micro-scaled architectures. This technique has been used before by Wang et al. [14,15] to fabricate carbon electrodes for micro-batteries. Typical glassy carbon consists of embedded closed pores, which can be opened by an appropriate activation process, such as thermal activation and electrochemical activation [16–18]. In this study, the capacitive properties of as-prepared C-MEMS micro-electrode arrays were investigated. To improve the performance of the C-MEMS structures, electrochemical activation was employed. Cyclic voltammetry (CV) and galvanostatic charge–discharge experiments were conducted to evaluate electrochemical performance of the activated micro-electrodes. The capacitive performances of activated and non-activated micro-electrode arrays were compared.

2. Experimental

2.1. Preparation of C-MEMS electrodes

The C-MEMS electrodes used in this study were prepared by a two-step photolithography process followed by a pyrolysis step. The substrate was SiO_2 (2000 Å)/Si and two kinds of negative tone photoresists, NANO^{TM} SU-8 25 and SU-8 100 (MicroChem Corp.), were used for the lithography process. In each step, development was carried out using a NANO^{TM} SU-8 developer (MicroChem Corp.). All other chemicals were purchased from Sigma–Aldrich. UV lithography was performed using an OAI 800 mask aligner. Detailed fabrication steps of C-MEMS structures are schematically presented in Fig. 1(a). In brief, a two-dimensional interdigitated finger pattern was firstly created using the photolithography of SU-8 25 photoresist. SU-8 25 was spin coated on the substrate with an initial speed of 500 rpm and then accelerated to 3000 rpm and kept for 30 s. Then, the spin coated photoresist was baked for 3 min at 65 °C and 7 min at 95 °C on a leveled hotplate. The baked photoresist was patterned with a UV exposure dose of 300 mJ cm^{-2}. Post-exposure bake was done for 1 min at 65 °C and 5 min at 95 °C on a leveled hotplate. Next, another photolithography process was employed using the SU-8 100 photoresist to create cylindrical posts on patterned fingers. In this step of the process, SU-8 100 was first spin coated on a finger patterned substrate, where a speed of 500 rpm was chosen to spread the photoresist, after which the speed was increased to 1500 rpm and kept at this speed for 30 s. Spin coated photoresist was then baked for 10 min at 65 °C and 45 min at 95 °C in an oven. The exposure was done using a UV exposure dose of 700 mJ cm^{-2}. Post-exposure bake was performed for 3 min at 65 °C and 10 min at 95 °C in an oven. Then the sample was developed in the SU-8 developer. Finally, the resulting SU-8 structures were pyrolyzed at 1000 °C for 1 h in forming gas atmosphere (i.e., 95% nitrogen and 5% hydrogen). To remove the residual carbon between the fingers after pyrolysis, all samples were subjected to oxygen plasma treatment at 400 mTorr with a power of 150 W for 20 s prior to other experimental investigations. After plasma treatment, electrical resistance between the interdigitated electrodes was measured and the resistance in the order of mega Ohms was confirmed. The total numbers of samples which are used for different characterization methods were 28 interdigitated C-MEMS micro-electrode arrays (schematically shown in Fig. 1(b)).

2.2. Electrochemical activation

To perform electrochemical activation on both electrodes of each C-MEMS micro-capacitor, the two electrodes were connected together through the contact pads (schematically shown in Fig. 1(b)) with a piece of silver wire. Then the contact pads and the silver wire were fully covered by epoxy resin to prevent their exposure to the electrolyte. Subsequently, the sample was composed into a three-electrode system as the working electrode. The reference and the counter electrodes were Ag/AgCl and a Pt wire, respectively. Electrochemical activation was performed in 0.5 M H_2SO_4 solution deaerated by nitrogen bubbling. A voltage of 1.9 V was applied to the electrodes for the durations of either 10 or 30 min using a multichannel potentiostat/galvanostat (VMP3, Princeton Applied Research). The electrodes were then negatively polarized at −0.3 V for 10 min. After electrochemical pretreatment, the electrodes were washed with DI water.

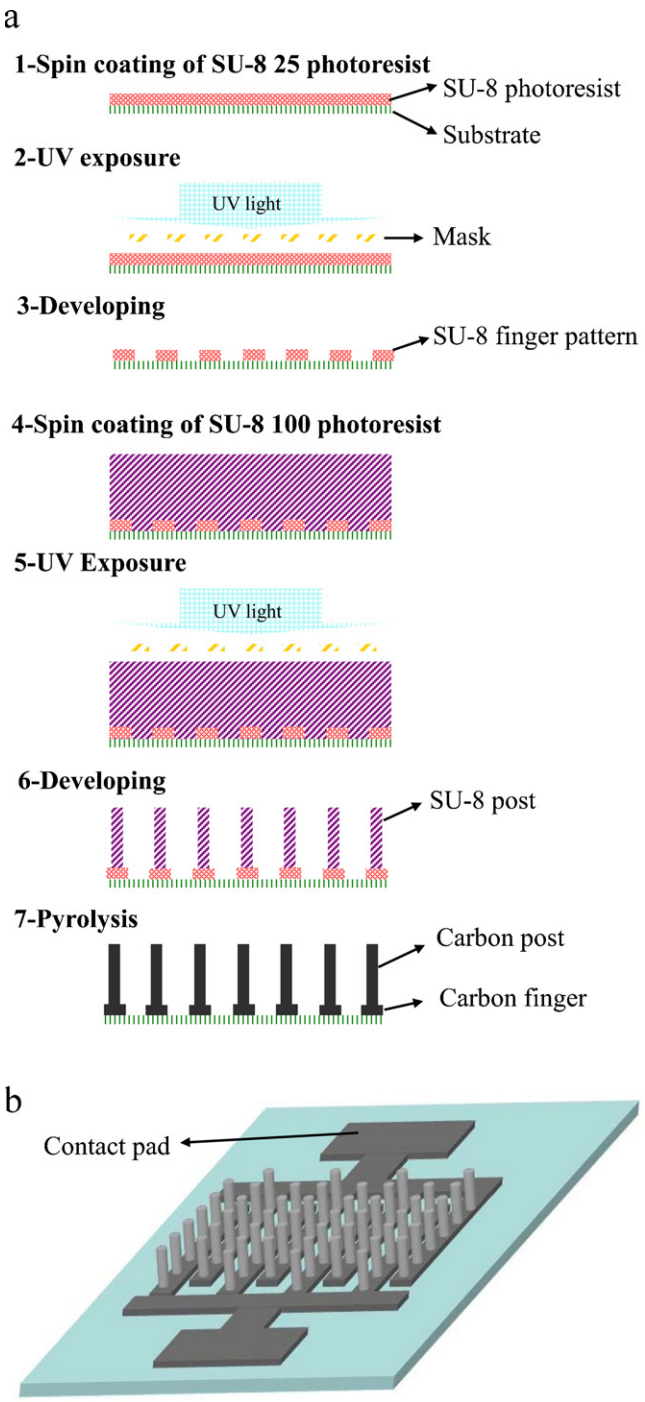

Fig. 1. (a) Schematic of a typical process flow for fabricating C-MEMS electrodes. (b) Schematic 3D view of a sample after carbonization.

2.3. Characterization

The microstructure of electrodes was investigated by a JOEL 6335 field-emission scanning electron microscope (FE-SEM). Electrochemical performance tests were performed in two-electrode electrochemical cells, where one of the interdigitated electrodes acted as the working electrode and the other as the counter electrode. The electrolyte was deaerated 0.5 M H_2SO_4 aqueous solution. CVs were recorded at different scan rates ranging from 5 to 200 mV s^{-1}. Galvanostatic charge/discharge experiments were performed under various current densities in the voltage range between 0 and 1 V. All the electrochemical tests were carried out in room temperature.

For each sample, geometric surface area and volume were measured using SEM and optical microscope images. The density of the photoresist-derived carbon was measured by calculating the weight of 5 carbon films with known thickness and geometric area. The average density was 1.52 g cm^{-3}. The weight of each electrode was estimated by multiplying the geometric volume by the average density of photoresist derived carbon. To confirm the accuracy of measured weights by this method, weights of 5 electrodes were measured by subtracting the measured weight before and after the removal of the electrodes from the substrate. The measured weights by the two methods were in good agreement and the average deviation in calculated weights was about 5%.

In this work, three different terms were used to describe the corresponding capacitance of the electrodes. For each electrode, specific gravimetric capacitance, specific geometric capacitance and specific volumetric capacitance is the capacitance of the electrode normalized by its mass, geometric surface area and volume, respectively.

3. Results and discussion

3.1. Structural characterizations

Fig. 2 shows typical SEM micrographs of C-MEMS electrodes. Carbon posts are perfectly aligned on carbon fingers and the device has two interdigitated 3D electrodes. The total footprint area of a typical sample was 9 mm × 9 mm with a total of 50 interdigitated fingers (25 fingers for each electrode) and the finger widths were ~100 μm. After carbonization, the measured post diameters of samples ranged from about 53 to 68 μm. The heights of carbon posts of different samples varied from about 115 to 140 μm with an average of ~130 μm. The origin of variation of post height and diameter for different samples is attributed to the difference in wafer chip size and small variations of the amount of photoresist used for spin coating during fabrication of each sample. We predict that the dimensions of carbon post for different samples can be effectively controlled by optimizing experimental parameters during the fabricating process. Due to the good adhesion of SU-8 25 to the substrate, the shrinkage of fingers during carbonization is less than the posts. On the other hand, the adhesion of SU-8 fingers and posts are also very good. Therefore, the shrinkage of the structure in contact regions of fingers and posts are controlled by the shrinkage of fingers. As a result, the posts have shrunk less near the base of the structures than at the midsection [14].

3.2. Electrochemical tests

3.2.1. Non-activated samples

CV was used to determine the electrochemical properties of the non-activated samples. Fig. 3(a) shows the CV curves of a non-activated sample at various scan rates. The CV curves show a near rectangular shape at all scan rates. The average current is low, ranging from 3.48 to 2.84 μA at 5 mVs^{-1}, and increases by increasing the scan rate. The capacitance of the two electrode cells can be calculated according to the following equation [19,20]:

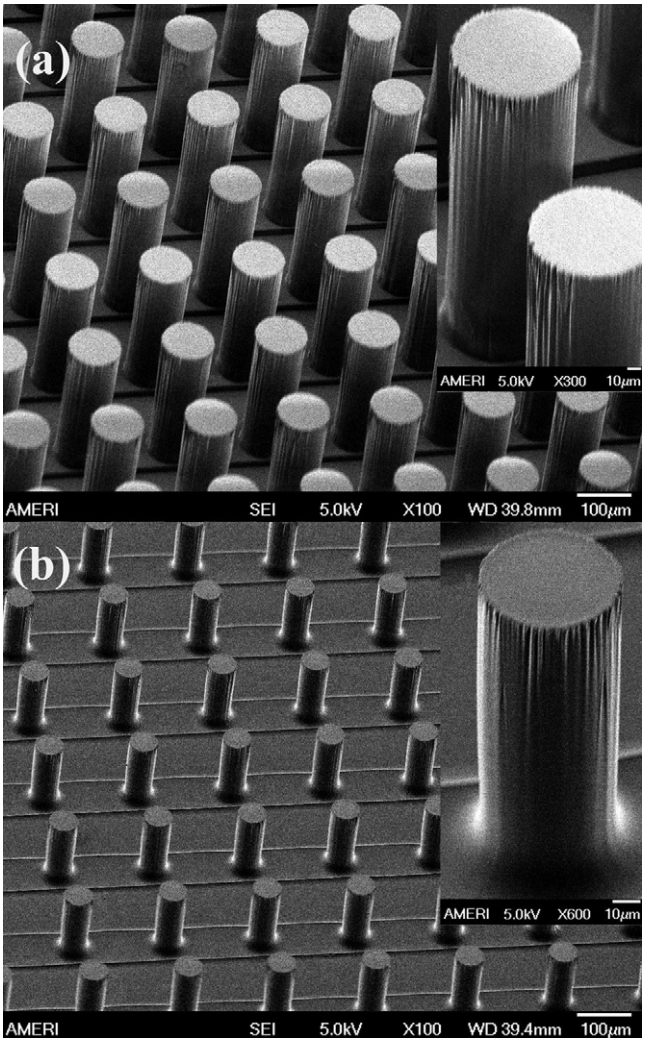

Fig. 2. SEM images of (a) SU-8 structure and (b) carbonized structure. The insets show higher magnification images.

$$C = \frac{\int I(V)\,dV}{2s\Delta V} \quad (1)$$

where $\int I(V)\,dV$ is the total voltammetric charge obtained by the integration of positive and negative sweep in cyclic voltammograms, s is the scan rate and ΔV is the width of the potential window. The capacitance calculated from Eq. (1) is the total capacitance of the cell which is the sum of the two equivalent single electrode capacitors in the series. To calculate the specific gravimetric and geometric capacitance of each electrode, Eqs. (2) and (3) have been used respectively.

$$C_m = \frac{2C}{m} \quad (2)$$

$$C_A = \frac{2C}{A} \quad (3)$$

where C_m is the specific gravimetric capacitance, C is the total capacitance of the cell, m is the mass, C_A is the specific geometric capacitance and A is the total geometric surface area of a single electrode. The two electrodes of the device have identical design specifications and have been fabricated simultaneously during the fabrication process. Moreover, the electrodes were activated at the

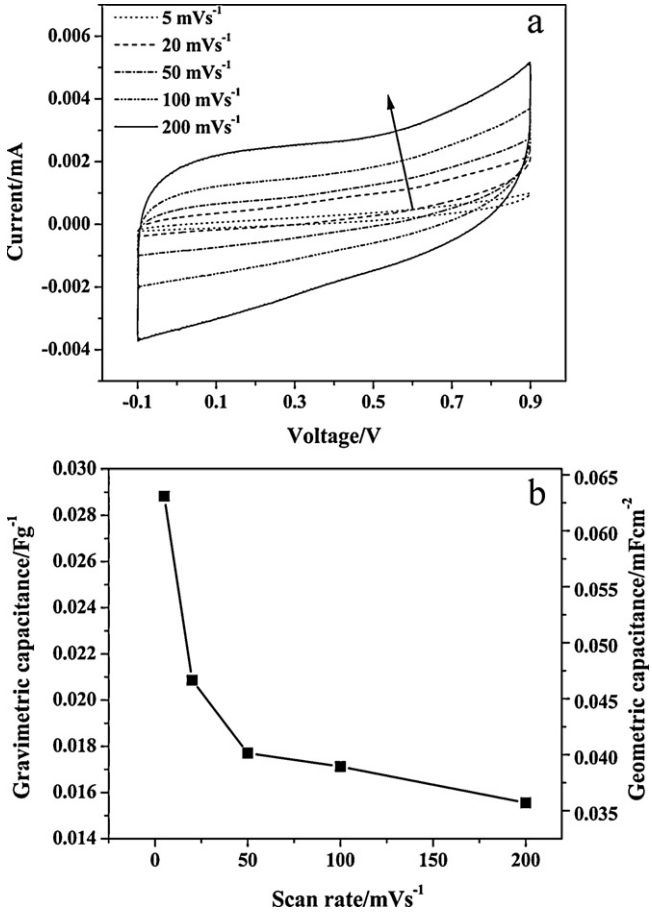

Fig. 3. (a) CVs of a non-activated sample (the arrow shows the direction of increasing scan rate). (b) The specific gravimetric and geometric capacitance of a non-activated sample at various scan rates.

same time in one electrochemical cell. Therefore, for calculating the capacitance, we have assumed that the two electrodes of the device have identical capacitance values.

Fig. 3(b) shows the specific gravimetric and geometric capacitances of C-MEMS electrodes measured at different scan rates of 5, 20, 50, 100, and 200 mV s^{-1}. The specific capacitance decreases gradually by increasing the scan rate and the highest value of geometric capacitance of ~0.07 mF cm^{-2} is found at the lowest scan rate of 5 mV s^{-1}. At this scan rate the specific gravimetric capacitance is calculated as ~0.03 F g^{-1}. Considering the relatively smooth and pore-free surface of the photoresist derived carbon structures, the low specific capacitance of as-pyrolysed C-MEMS electrodes is reasonable [21]. This implies the active surface of these electrodes is limited to their measurable geometric surface.

3.2.2. Electrochemically activated samples

Fig. 4(a) presents the CV curves at different scan rates of a sample activated for 30 min. The curves at all scan rates show a near rectangular shape and a broad band was observed on top of these rectangular responses. It is known that the anodic oxidation of samples increases the amount of oxygen groups on the electrode surface [17]. A broad peak at 0.2–0.4 V during the anodic sweep can be attributed to the contribution of active oxygen surface groups generated by electrochemical treatment [22]. CV studies of electrochemically activated glassy carbon by Nagaoka and Yoshino also show a similar broad peak on anodic curves [23]. In addition, the shapes of anodic/cathodic sweeps are asymmetric, which is in accordance with the reports by Sullivan et al. [17,22] and Nagaoka and Yoshino [23]. This is due to either slow electron transfer between surface redox-active groups and the bulk glassy carbon, or charging effects resulting from small pores and microcracks [17,22,23].

In Fig. 4(b) CV curves of a non-activated sample and a sample activated for 30 min are compared at the same 100 mV s^{-1} scan rate. The area of the activated sample's CV curve is significantly larger

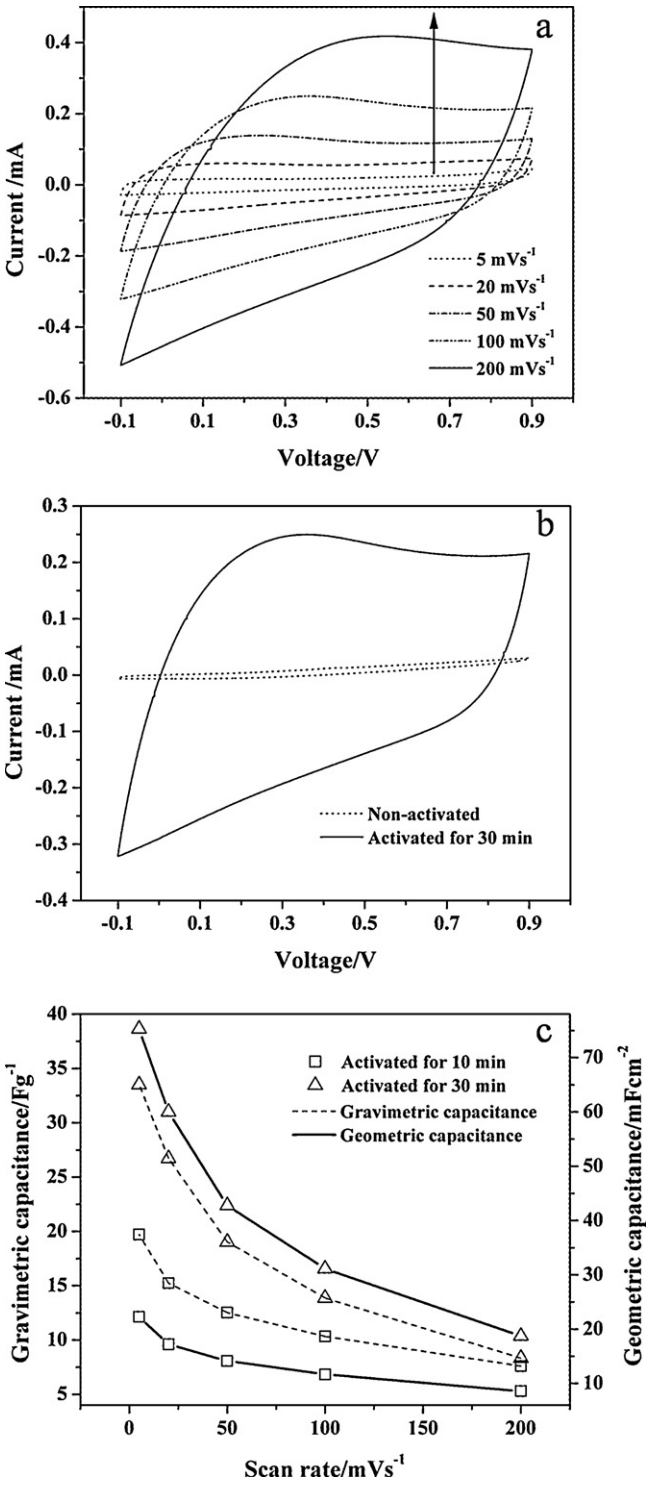

Fig. 4. (a) CVs of microelectrodes in two-electrode cells after activation for 30 min at different scan rates (the arrow shows the direction of increasing scan rate). (b) Typical CVs of samples before and after activation for 30 min in 0.5 M H_2SO_4 aqueous electrolyte at 100 mV s^{-1} scan rate. (c) The specific gravimetric and geometric capacitance of activated samples at various scan rates.

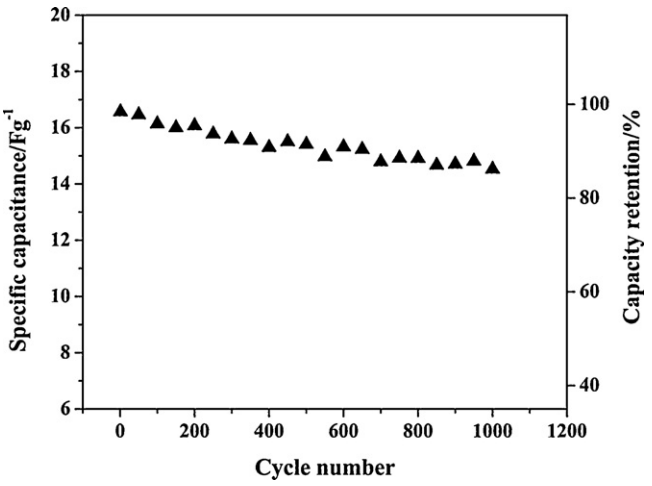

Fig. 5. Cyclic performance and capacity retention for an activated sample.

than that of the non-activated sample, which implies the enhancement of the specific capacitance after activation. The gravimetric and geometric specific capacitance of samples activated for 30 min and 10 min were calculated from CV curves (shown in Fig. 4(c)). For all samples, the specific capacitance decreases with an increase in the scan rate. The specific gravimetric capacitance of the sample activated for 30 min ($\sim$33 F g^{-1}) was almost three orders of magnitude higher than the non-activated sample ($\sim$0.03 F g^{-1}). At a scan rate of 5 mV s^{-1}, the geometric capacitance for the non-activated and activated (30 min) samples was $\sim$0.07 mF cm^{-2} and $\sim$75 mF cm^{-2}, respectively. The geometric capacitance of the sample activated for 10 min was $\sim$22 mF cm^{-2}. At the same scan rate, the volumetric capacitance of samples activated for 10 and 30 min was $\sim$14 F cm^{-3} and $\sim$48 F cm^{-3}, respectively. The specific capacitances at different scan rates of the sample activated for 30 min are higher than that of samples activated for 10 min at corresponding scan rates.

The C-MEMS sample activated for 30 min was also examined by CV tests for 1000 cycles at the scan rate of 50 mV s^{-1} in the two electrode system. The capacitance value has been plotted and shown in Fig. 5. The specific capacitance of this sample at the first cycle was $\sim$17 F g^{-1}. After 1000 cycles, the specific capacitance was 15 F g^{-1} and there was only 12.3% fade of the initial capacitance. This indicates acceptable cyclability of activated micro-electrodes compared to electrochemical micro-capacitors reported by Lim et al., where 53% of the initial capacitance faded after 500 cycles [4].

In order to further investigate the performance of electrochemically activated C-MEMS micro-electrodes, galvanostatic charge/discharge experiments were performed on activated samples with various current densities in a voltage range of 0–1.0 V. Examples of charge/discharge curves of the samples activated for 30 min at various discharge current densities are shown in Fig. 6(a). The charging half of each charge/discharge cycle is almost a straight line when excluding the initial *iR* drop. The discharge curves also have small *iR* drops at the beginning as shown in Fig. 6(a). After the *iR* drop, the decrease of voltage with increasing time deviates from a straight line. Deviation from ideality in voltage–time curves has also been observed for electrochemically modified graphite electrodes by Xu et al. [24]. Niu et al. [25] also reported non-linearity in voltage–time curves of porous C-cloth material. While pseudo-capacitive contribution from redox-active surface groups can cause the deviation from linearity in charge/discharge curves, Niu et al. [25] explained that other factors may also contribute to this non-ideal behavior. These factors include redistribution of charge within the pores of activated electrodes during charging or discharging and the effect of direct equivalent series resistance (ESR). The discharge capacitance of the cell was measured from the discharge curves after the *iR* drop, according to the following equation [26]:

$$C = I \times \Delta t \times \Delta V^{-1} \quad (4)$$

where I is the current and Δt is the time interval for the change in voltage range ΔV. The specific gravimetric and geometric capacitance of the electrodes was calculated using Eqs. (2) and (3), respectively.

Fig. 6(b) shows the variation of the specific gravimetric and geometric capacitance of activated samples at various discharge rates. The geometric capacitance is $\sim$48 mF cm^{-2} at 1 mA cm^{-2}. Specific gravimetric capacitance decreases from $\sim$24 F g^{-1} at 0.5 mA cm^{-2} discharge current density to $\sim$11 F g^{-1} at 5 mA cm^{-2} discharge current density. These results are in agreement with the above CV results.

The improvements in electrochemical performance of activated electrodes can be explained by the following reasons. Firstly, introducing oxygen groups to the surface carbon electrodes is able to improve the wettability of the electrode surface and contribute additional pseudo-capacitance [27]. While the appearance of a current maximum on CV curves (Fig. 4(a)) proves the existence of oxygen groups on the surface of the electrodes, further studies need to be done to quantitatively evaluate their contribution to the capacitive performance of the electrodes. Secondly, the increase in the surface area of the electrodes after activation seems to be

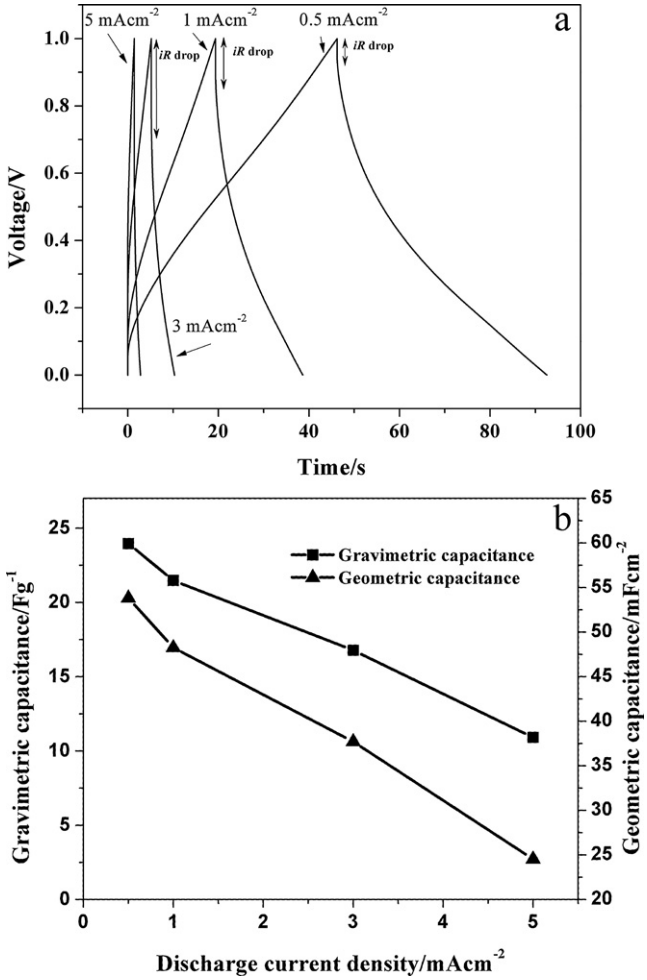

Fig. 6. (a) Galvanostatic charge/discharge curves at various discharge rates. (b) The specific gravimetric and geometric capacitance of activated samples at various discharge rates. The sample was electrochemically activated for 30 min.

the main reason of enhancement of specific capacitance since the electrochemical pretreatment oxidizes the carbon surface and thus opens up the internal closed pores, which is demonstrated by Sullivan et al. [22]. Braun et al. [28] had suggested that this activation process creates a large and electrochemically accessible internal surface area, which thus increases the double layer capacitance. Our attempts to analyze the pore size of the electrodes by studying gas adsorption isotherms could not deliver reliable results mainly because the small amount of active materials for each micro fabricated sample makes it impossible to have a precise sorption measurement. Further investigations need to be done in order to quantify the increase in surface area of the electrodes after electrochemical activation.

Another possible reason for the increase in the capacitance of the electrodes after electrochemical treatment is the irreversible intercalation of ions during polarization. This phenomenon has been observed for graphitizable carbon [29]. It is reported that, during the first polarization cycle ions are inserted into the carbon structure. This intercalation process is irreversible and provides a larger specific capacitance in successive cycles [29]. To investigate intercalation in C-MEMS electrodes, we performed polarization on electrodes for several cycles (between 0 and −2.5 V). No significant irreversible increase in the capacitance was observed for the C-MEMS electrodes.

Compared to previously published works on carbon based electrochemical micro-capacitors [9,10], our micro-capacitors based on C-MEMS shows excellent and promising performance. Despite the significant improvement after electrochemical activation, the gravimetric capacitance of the C-MEMS electrode is still lower than that of activated carbon powders with very high BET surface area which is widely used in ECs. It was reported that KOH activated carbon with a BET surface area of 3150 $m^2 g^{-1}$ shows specific gravimetric capacitance of 312 $F g^{-1}$ in a 1 M H_2SO_4 solution [30]. This can be reasonable considering the activation mechanism during electrochemical activation. As mentioned above, electrochemical activation forms an active porous film on the surface of the electrode. Braun et al. [28] showed that the formation of the active film begins at the outer surface of the carbon and extends into the interior gradually during the activation process, surrounding an inactive core with closed pores. The thickness of the active layer linearly increases with an increase in the activation time as reported by Sullivan et al. [22]. For the activation time of 30 min used in this study, we can expect the thickness of the active film to be just a few microns. This indicates that a carbon layer with a thickness of only a few microns on the surface of carbon posts contribute to the capacitance of electrodes, and a large amount of the mass of the electrode is not accessible to the electrolyte. It is assumed that by increasing the surface area and decreasing the mass of electrodes through fabrication of high aspect ratio carbon posts, the gravimetric specific capacitance can be improved. Furthermore, as projected from Fig. 4(c) electrochemical activation of electrodes for longer durations could result in a further increase in the specific capacitance of samples. Moreover, based on the proposed model of development of porous structures on the surface of glassy carbon electrodes by Sullivan et al. [22] and Braun et al. [16], we can assume that at the initial stages of activation, the pore entries are too small for the electrolyte to penetrate. As activation advances, pore walls would be thinned, and thus pores will grow in size. Therefore, increasing the activation time will also enhance the accessibility of the pores, which in turn enhances the electrochemical capacitance of the electrodes under high charge–discharge current conditions. Enhancement of the accessibility of the electrolyte will also improve the non-ideal behavior which was observed in the voltage–time curve. Our attempts to further increase the activation time is not repeatable since the carbon current collectors (fingers) delaminated from the surface of the wafer in the case of longer activation times. Further research is underway to improve the adhesion of carbon fingers to the substrate.

The present study demonstrates that C-MEMS fabricated interdigitated micro-electrodes are potentially capable of delivering energy storage solutions for micro-devices. Compared to as-prepared electrodes, electrochemical activation of electrodes for 30 min increased the capacity by three orders of magnitude. Fabrication of higher aspect ratio micro-electrodes can increase the surface area of the device in the limited footprint area thus increasing the capacitance normalized by the footprint of the device. Future developments will include fabrication of higher aspect ratio 3D electrodes, increasing the adhesion of carbon current collectors to the substrate, and optimizing the conditions of electrochemical activation.

4. Conclusion

The C-MEMS technique was used to fabricate interdigitated micro-electrode arrays for on-chip electrochemical micro-capacitors. Electrochemical characterization of electrochemically activated micro-electrodes shows excellent capacitive behavior. Specific geometric capacitance of ~75 mF cm^{-2} was achieved after electrochemical activation for 30 min. For this activation duration the volumetric capacitance was ~48 F cm^{-3}. These results indicate that the C-MEMS technique is a very promising method for the fabrication of electrochemical micro-capacitors. However, the non-ideal voltage–time curves and rapid drop in capacitance at high scan rates suggests that activation conditions should be improved to enhance the electrochemical properties of micro-devices.

Acknowledgments

We acknowledge the financial support of the US Defense Advanced Research Projects Agency (DARPA) Young Faculty Award program (Project No. HR0011-08-1-0036). We also acknowledge the National Science Foundation (MRI program CMMI-0821582) and American Chemical Society Petroleum Research Fund (49301-0N110). The authors further thank the AMERI staff of FIU for their clean-room facilities.

References

[1] F. Albano, Y.S. Lin, D. Blaauw, D.M. Sylvester, K.D. Wise, A.M. Sastry, J. Power Sources 185 (2008) 1524–1532.
[2] J.D. Morse, Int. J. Energy Res. 31 (2007) 576–602.
[3] K.A. Cook-Chennault, N. Thambi, A.M. Sastry, Smart Mater. Struct. 17 (2008) 043001.
[4] J.H. Lim, D.J. Choi, H.K. Kim, W.I. Cho, Y.S. Yoon, J. Electrochem. Soc. 148 (2001) A275–A278.
[5] B.E. Conway, W.G. Pell, J. Solid State Electrochem. 7 (2003) 637–644.
[6] P. Simon, Y. Gogotsi, Nat. Mater. 7 (2008) 845–854.
[7] J.-W. Sung, S.-J. Kim, K.-H. Lee, J. Power Sources 133 (2004) 312–319.
[8] W. Sun, X. Chen, J. Power Sources 193 (2009) 924–929.
[9] M. Kaempgen, C.K. Chan, J. Ma, Y. Cui, G. Gruner, Nano Lett. 9 (2009) 1872–1876.
[10] D. Pech, M. Brunet, P.-L. Taberna, P. Simon, N. Fabre, F. Mesnilgrente, V. Conédéra, H. Durou, J. Power Sources 195 (2010) 1266–1269.
[11] C. Wang, R. Zaouk, B.Y. Park, M.J. Madou, Int. J. Manuf. Technol. Manage. 13 (2008) 360–375.
[12] C. Wang, G. Jia, L.H. Taherabadi, M.J. Madou, J. Microelectromech. Syst. 14 (2005) 348–358.
[13] H. Xu, K. Malladi, C. Wang, L. Kulinsky, M. Song, M.J. Madou, Biosens. Bioelectron. 23 (2008) 1637–1644.
[14] C. Wang, L. Taherabadi, G. Jia, M. Madou, Y. Yeh, B. Dunn, Electrochem. Solid-State Lett. 7 (2004) A435–A438.
[15] J.W. Long, B. Dunn, D.R. Rolison, H.S. White, Chem. Rev. 104 (2004) 4463–4492.
[16] A. Braun, M. Bärtsch, O. Merlo, B. Schnyder, B. Schaffner, R. Kötz, O. Haas, A. Wokaun, Carbon 41 (2003) 759–765 (it was 14 before).
[17] M.G. Sullivan, B. Schnyder, M. Bärtsch, D. Alliata, C. Barbero, R. Imhof, R. Kötz, J. Electrochem. Soc. 147 (2000) 2636–2643.
[18] A. Dekanski, J. Stevanovic, R. Stevanocic, B.Z. Nikolic, V.M. Jovanovic, Carbon 39 (2001) 1195–1205.

[19] H. Li, J. Wang, Q. Chu, Z. Wang, F. Zhang, S. Wang, J. Power Sources 190 (2009) 578–586.
[20] B.E. Conway, Electrochemical Supercapacitors: Scientific Fundamentals and Technological Applications, Kluwer, New York, 1999.
[21] A. Singh, J. Jayaram, M. Madou, S. Akbar, J. Electrochem. Soc. 149 (3) (2002) E78–E83.
[22] M.G. Sullivan, R. Kötz, O. Haas, J. Electrochem. Soc. 147 (2000) 308–317.
[23] T. Nagaoka, T. Yoshino, Anal. Chem. 58 (1986) 1037–1042.
[24] H. Xu, X. Fan, Y. Lu, L. Zhong, X. Kong, J. Wang, Carbon 48 (2010) 3293–3311.
[25] J. Niu, W.G. Pell, B.E. Conway, J. Power Sources 156 (2006) 725–740.
[26] J. Wang, Y. Xu, X. Chen, X. Du, J. Power Sources 163 (2007) 1120–1125.
[27] E. Frackowiak, Phys. Chem. Chem. Phys. 9 (2007) 1774–1785.
[28] A. Braun, J. Kohlbrecher, M. Bärtsch, B. Schnyder, R. Kötz, O. Haas, A. Wokaun, Electrochim. Acta 49 (2004) 1105–1112.
[29] P.W. Ruch, M. Hahn, D. Cericola, A. Menzel, R. Kötz, A. Wokaun, Carbon 48 (2010) 1880–1888.
[30] K. Kierzek, E. Frackowiak, G. Lota, G. Gryglewicz, J. Machnikowski, Electrochim. Acta 49 (2004) 515–523.